§ sciendo

Capabilities of Thomson parabola spectrometer in various laser-plasma- and laser-fusion-related experiments

Przemysław Tchórz ⓘD,
Maciej Szymański ⓘD,
Marcin Rosiński ⓘD,
Tomasz Chodukowski ⓘD,
Stefan Borodziuk ⓘD

Abstract. The Thomson parabola spectrometer (TPS) [1] is a well-known, universal diagnostic tool that is widely used in laser plasma experiments to measure the parameters of accelerated ions. In contrast to other popular ion diagnostics, such as semiconductor detectors or ion collectors, the TPS is not greatly affected by electromagnetic pulses generated during high-power laser interaction with matter and can be tuned to acquire data in various energy ranges of accelerated ions, depending on the goal of the experiment. Despite the many advantages of this diagnostic device, processing the collected data is a difficult task and requires a lot of caution during interpretation of gathered results. In this work, we introduce the basic principles of operation and data analysis based on the numerical tool created specifically for the TPS designed at the Institute of Plasma Physics and Laser Microfusion, present a range of data obtained during various recent experiments in which our TPS was used, and highlight the difficulties in data analysis depending on the purpose of the experiment and the experimental setup.

Keywords: Acceleration • Diagnostic • Ion • Laser • Plasma • Thomson spectrometer

P. Tchórz✉, M. Szymański, M. Rosiński,
T. Chodukowski, S. Borodziuk
Institute of Plasma Physics and Laser Microfusion
Hery 23 St., 01-497 Warsaw, Poland
E-mail: przemyslaw.tchorz@ifpilm.pl

Introduction

An experimental approach to laser ion acceleration [2] requires the use of a wide range of diagnostic devices to provide information about both accelerated ions and secondary products of the aforementioned process, such as X-ray emission or gamma ray emission [3]. The most popular detectors used in this kind of research are based on semiconductor structures and provide time-of-flight (TOF) information, which allows one to calculate the energies and quantities of accelerated ions with respect to the beginning of the interaction, which is indicated by a so-called photopeak, related to the electromagnetic waves approaching the detector [4] . However, the photopeak itself, as well as the electromagnetic pulses (EMPs) [5] generated during laser–matter interaction, very often affects the actual measurement in a disruptive or even destructive way, which causes the loss of information. Therefore, using additional diagnostic devices is required for both consistency and cross-calibration of obtained data. Moreover, the ion beams accelerated during the laser ion acceleration process have a multi-ion nature; therefore, distinction of different accelerated ion species plays a crucial role in understanding the physics of laser–matter interaction. There are numerous commonly used diagnostic tools for this purpose; however, the most universal device for this

kind of ion beam characterization is the Thomson parabola spectrometer (TPS). The TPS provides information about the energy, momentum, and charge-to-mass ratio of the accelerated particles. Contrary to semiconductor detectors (sensitive to energies in the range of >1 MeV) and ion collectors (usually used for characterizing low-energy ions, <1 MeV), the data acquisition process in the TPS is rarely affected by the EMP and can be reliably used for a wide energy spectrum of accelerated ions. In this work, we summarize recent improvements and achievements in using the TPS during particular laser-plasma-related experiment and highlight both advantages and limitations of this diagnostic tool in the following sections.

Design of Thomson parabola spectrometer

The TPS is a widely used and well-known device that uses magnetic and electric fields (Eq. (1)) to deflect accelerated ions, which then can be registered on either passive (CR-39, track detector, imaging plate) or active (multichannel plate and camera setup) medium in the form of parabolas corresponding to ion species with different charge-to-mass ratios (Fig. 1).

$$(1) \qquad \vec{F} = q\overrightarrow{E_{EL}} + q\left(\vec{v} \times \vec{B}\right)$$

The standard design of the TPS assumes parallel electrodes, which ensure that the electric field is constant over the length of the field $\vec{E}$. In this case, under the influence of a constant magnetic field $\vec{B}$, parallel to the electric field $\vec{E}$, the deflection of the particle can be described by Eqs. (2) and (3), respectively [6]:

$$(2) \qquad D_B = \frac{qBL_B}{mv_Z}\left(\frac{1}{2}L_B + d_B\right)$$

$$(3) \qquad D_E = \frac{qEL_E}{mv_Z^2}\left(\frac{1}{2}L_E + d_E\right)$$

where D_B and D_E are the deflections caused by the magnetic and electric fields, respectively, and q, m, and v_Z are the charge, mass, and velocity components along the axis of the spectrometer body.

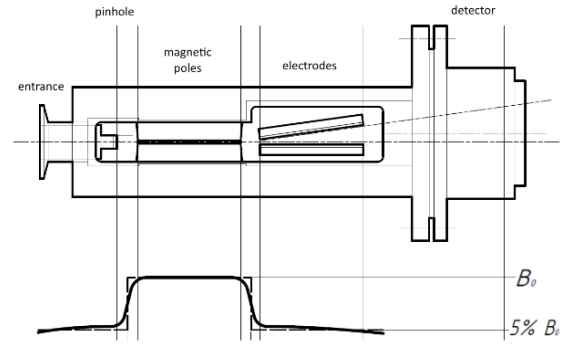**Fig. 1.** Parabolas registered on a microchannel plate coupled with a phosphor screen.

Fig. 2. Schematic representation of the TPS developed in the Institute of Plasma Physics and Laser Microfusion.

Moreover, L_E and L_B are the lengths over which the electric and magnetic fields are applied, and d_E and d_B stand for the distances between the detector plane and the end of the $\overrightarrow{E_{EL}}$ and $\vec{B}$ fields.

With the recent increase of available laser intensities, which allow to accelerate ions to energies reaching up to tens of mega-electron volts (MeVs) [7], the crucial TPS parameters that affect data acquisition and processing are the dispersion of deflecting fields and energy resolution. Deflecting such energetic ions would require tens of kilovolts of voltage to generate an electric field strong enough to provide sufficient separation of parabolic traces, and at the same time, preserving information about less-energetic particles would not be possible. Therefore, efforts have been made to develop novel variants of the TPS that would be more suitable for experiments that involve ultraintense laser pulses [8, 9].

The spectrometer developed in the Institute of Plasma Physics and Laser Microfusion (IPPLM) (Fig. 2) is designed as a separate unit with its own pumping system. This allows differential pumping, so that a higher level of vacuum can be obtained in the spectrometer chamber than in the interaction chamber. This is especially important when using the microchannel plate (MCP) as the particle detector. This type of detector requires vacuum in the order of 10^{-5} hPa for safe operation, which – in some cases – cannot be achieved in the main chamber. The spectrometer is connected to the interaction chamber by means of the flexible bellows and the standard KF40 interface. This allows the use of extension tubes between the chamber and the spectrometer, as well as installation of TOF diagnostics (semiconductor detectors or ion collectors) on the same line of sight.

The ion beam entering the spectrometer is formed by means of a single pinhole mounted in the special holder installed in the entrance port of the spectrometer. The holder made of aluminum alloy is designed in such a way as to block the stray light from the interaction chamber, attenuate the X-rays, and reduce the molecular gas conductance to increase the differential pumping efficiency.

Additionally, a special KF40 centering ring is used between the spectrometer chamber and the gate valve made of 10-mm-thick stainless steel with only a 3-mm hole in the center, to attenuate the X-rays from the plasma contributing to the detector background and limiting its bandwidth.

Depending on the application, various types of pinholes of sizes ranging from 200 μm to 450 μm are used. The pinhole size must be carefully selected to find the best compromise between resolution (calling for the smallest possible size) and detector signal (a bigger pinhole allows detection of the less--abundant ion species but also may cause detector saturation for the abundant ones).

The pinhole design is also crucial for the definition of the zero point. X-rays passing though the pinhole material around the hole itself may lead to a large halo around the zero point, which makes the exact localization of the zero point difficult. This can be a source of significant error in the obtained energy spectra and even lead to wrong identification of ion species. Currently, the best results have been obtained with pinholes machined from brass with 1-mm-long drilled holes.

The separation system of the spectrometer follows the classical scheme with magnetic and electric separators located one after another, sharing some characteristics with the previous IPPLM design [10]. The electric subsystem consists of two deflecting plates in the tilted configuration proposed by Carroll *et al.* [6]. In this configuration, as compared to the traditional parallel deflection plate scheme, higher particle deflections can be achieved with much lower voltages (Fig. 3). In the case of the spectrometer designed in the IPPLM, voltages in the 2-kV range are used for registration of protons with up to 4-MeV energies. At this level of voltage, a single high-voltage power supply can be used with the second deflecting plate grounded (in most parallel plate systems, a pair of negative and positive power supplies is used). This simplifies the whole system and increases its portability.

The magnetic subsystem is located directly behind the pinhole and consists of two soft iron poles mounted inside the chamber and a pair of permanent magnets mounted from the outside. The poles are carefully shaped to minimize fringe fields and increase the uniformity of the deflecting field. Due to the placement of the separating subsystems one after another, the gap between the magnetic poles can be reduced to only 3 mm, leading to strong deflecting fields with the use of moderately strong magnets. A maximum field with mean induction of 167.6 mT can be obtained with a pair of $75 \times 50 \times 20$ mm ferrite magnets.
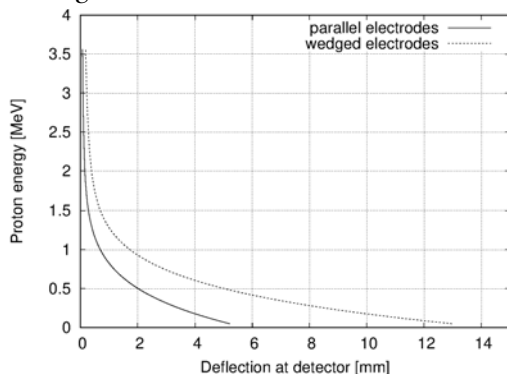

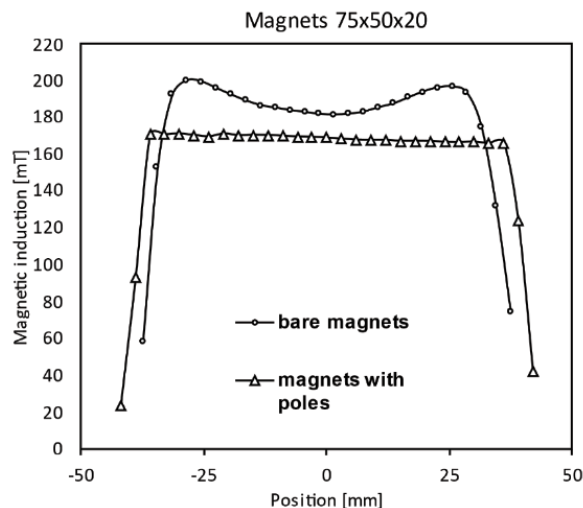**Fig. 3.** Dispersion curve for protons with wedged and parallel electrodes.

Fig. 4. Comparison of an example of the magnetic induction of bare magnets (glued) and magnets attached to poles, measured with a Hall probe.

The combination of soft iron poles and permanent magnets has many advantages. It eliminates the need for a bulky electromagnet, its high current supply, and overheating problems. The poles not only minimize the fringe field but also homogenize the field along the spectrometer. Measurements made with a Hall probe show that the magnetic induction between the poles has nearly constant value, with a well-defined sharp cutoff at the ends (Fig. 4). The bare magnets show high variation and strong edge effects, especially in the case of magnets glued together from smaller pieces. The poles also allow the use of magnets not matching the pole size. The field uniformity is still maintained along the whole poles. This is especially important when weak magnetic fields are used when the heavy, highly ionized particles are to be registered.

The detection system of the spectrometer is interchangeable and can be configured for the use of one of three types of detectors: the MCP, image plate (IP), or track detector.

The MCP, combined with the fluorescent screen and digital camera, is a very convenient type of detector as it offers the immediate registration of the particle tracks without any additional preparation or postprocessing. This fast acquisition capability combined with high sensitivity makes the MCP the detector of choice for analyzing ion spectra generated by low-energy, high-repetition-rate laser systems. It is used as the default detection system at the IPPLM 10 TW Pulsar femtosecond laser system. On the other hand, MCP requires a two-channel high-voltage power supply and relatively good vacuum to avoid gas breakdown and damage of the detector. Moreover, ions arriving at high quantities to the MCP may cause arcing over and damage of the detector.

The IPs constitute a well-established type of charged-particle-and-radiation detectors. The fact that the IP is a passive detector without any electronic components makes it a viable choice for medium- or high-energy, low-repetition-rate laser systems, where large amounts of ions and strong

electromagnetic pulses are encountered, rendering the electronic recording devices problematic. The drawback of the IP is that while, in contrast to X-ray films and nuclear emulsions, it does not require wet chemical processing, it still has to be removed after each shot and scanned in a dedicated scanner. Moreover, handling IPs calls for some attention as the active surface can be easily damaged, and the exposure to the sun or fluorescent lamps causes erasure of the recorded tracks. This makes this kind of detector of limited use in applications wherein high shot repetition rate is required.

The plastic track detectors (CR-39, Tastrak, UK) can be regarded as a supplementary diagnostic tool. The long processing time, combined with a complicated analysis procedure, prevents this kind of detector from being the first choice. However, the ability of distinguishing individual particle tracks and particle type identification may be a particularly important factor for the TPS. Because the spectrometer is not able to separate geometrically different ions with the same charge-to-mass ratio (e.g., the α particles and C^{6+} carbon ions), the use of a track detector can be a solution to this problem. It is worth noting that a small piece of the plastic track detector may be placed over the IP for differentiating particles in the region of interest, while the rest of the spectrum is recorded on the IP.

Numerical methods for data analysis

In contrast to a typical TPS construction with parallel electrodes, Eqs. (2) and (3) do not apply in this configuration because the electric field is not constant along the axis of particle propagation due to the wedge-like geometry of electrodes. Equations similar to Eqs. (2) and (3) could be solved. However, they are much more complicated than in the standard approach. Instead, taking advantage of the high computing power of modern-day central processing units (CPUs), we solve Eq. (1) numerically, iterating over the quadratic step of energy to calculate the trajectory of the particle with a given charge-to-mass ratio. The entry point for computing the theoretical parabola is the range of energies, defined by the maximum and minimum kinetic energies provided during the analysis. Based on that fact, the deflection in both vertical and horizontal directions is calculated, taking into consideration the strength of the fields and the geometry of the TPS chamber. The strength of the electric field between the wedged electrodes can be calculated using Eq. (4):

$$(4) \qquad E_{EL}(z) = \frac{U}{d(z)} = \frac{U}{A \cdot z + B}$$

$$A = \frac{d_2 - d_1}{Z e_2 - Z e_1}, \quad B = d_1 - AZ e_1$$

where d_2 and d_1 are, respectively, the distances between the plates at the beginning and the end of the electric separator; Ze_1 and Ze_2 are the beginning and the end of the electric separator in respect to the propagation axis z. This model assumes that the electric field linearly decreases along the electromagnet and that there is no electric field outside the plates. However, we assume that the magnetic field outside the magnetic deflection part is equal to 5% of $\vec{B}$, and has a parasitic influence on the magnetic deflection of ions. This assumption is based on the Hall probe measurements of the magnetic field inside the spectrometer chamber, but outside the magnetic deflection module.

The computed parabolic shape can be compared to experimental data (Fig. 5) and the intensity of pixels, proportional to the number and energy of registered particles, can be extracted. This procedure is repeated for all energies used in computing the parabola points, allowing the reconstruction of a qualitative energy distribution for a given ion species (Fig. 6), which is limited only by the dimensions of the detector; low-energy particles are deflected outside the active area and therefore information about them cannot be retrieved. Along with the energy spectrum, the synthetic TOF signal can be created, using the relative pixel intensity and recalculating the time of ion arrival at the detector from the energy distribution corresponding to a specific charge-to-mass ratio. Such information can be later compared with measurements made by the ion collector or the track detector placed near the TPS to cross-correlate the data.
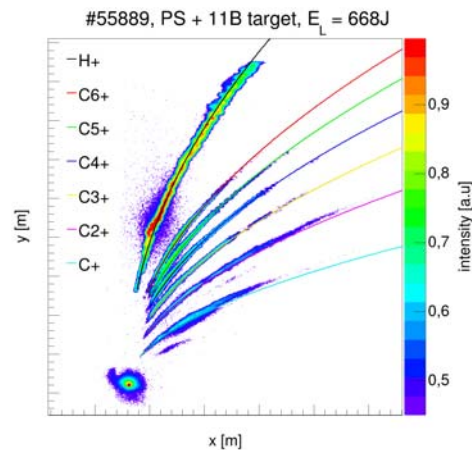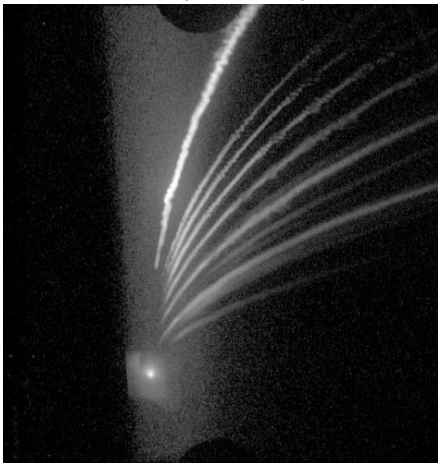

Fig. 5. Original scan from the IP (left) and the calculated parabolas fitted to the experimental proton and carbon lines (right). The chosen intensity threshold removed low-intensity parabolas from the pictures.
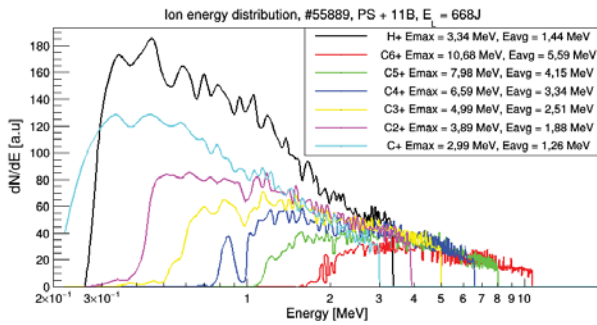
Fig. 6. Example of ion energy spectrum extracted from the IP (scan in Fig. 5).

Results and discussion

Our recent experiment at the PALS facility [11] was related to the cavity pressure acceleration (CPA) phenomena [12]. During the first part of the experimental study, an upgraded design of the cavity target from previous experiments (Fig. 7) was used to further increase the pressure and temperature inside the cavity to further accelerate the plasma jet escaping the target. The energy of the laser pulse was in the range of 200–700 J, and the pulse duration was equal to 400 ps at the wavelength of 1.315 μm.

The laser pulse had to be injected into the 20-μm--long channel of the cavity target and focused down to a minimal achievable (100 μm) focal spot in the correct region of the target cavity. The dimensions of the target were tailored to perfectly fit the geometry of the laser beam. Due to the complicated construction of the target, precise positioning of the target in respect to the fixed position of the laser pulse's focal spot was difficult and, in numerous shots, it did not provide proper laser–matter interaction results expected in this acceleration scenario.

Utilizing the TPS (pinhole: 300 μm, voltage: 3 kV, magnetic induction: 167 mT for the presented results) with the BAS-IP (TR) detector allowed us to not only measure the energy of the accelerated ions and obtain their energy spectra but also qualitatively determine the quality of laser focusing in the cavity during laser–matter interaction; proper interaction with the inner part of the cavity was recognized by the presence of the secondary trace of the parabola representing protons escaping the cavity by means of the CPA scheme.

The explanation for the clearly visible double proton parabolas is that there are two different sources of the registered ions. The primary source is the initial interaction with the inner part of the cavity, where the ions are accelerated in a well-known scenario of ablative acceleration [13]. Typical ion traces for this kind of interaction are visible in Fig. 8. In this case, the ion energy spectra obtained during our analysis match the usual results when thick (~1 mm), solid targets are used at the PALS facility (Fig. 10). In such cases, the CPA process did not occur, most likely due to the improper focusing of the pulse inside the cavity. The evidence of that is the lack
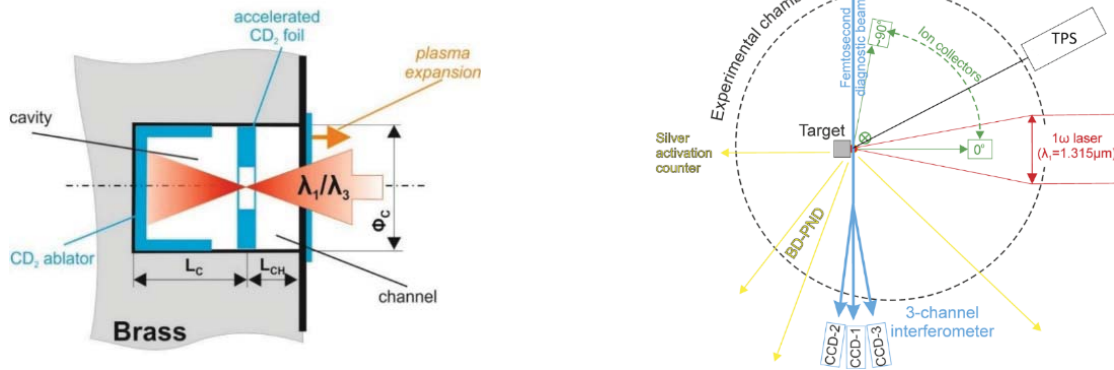

Fig. 7. Schematic of novel CPA target used in the experiment (left) and the experimental setup (right).
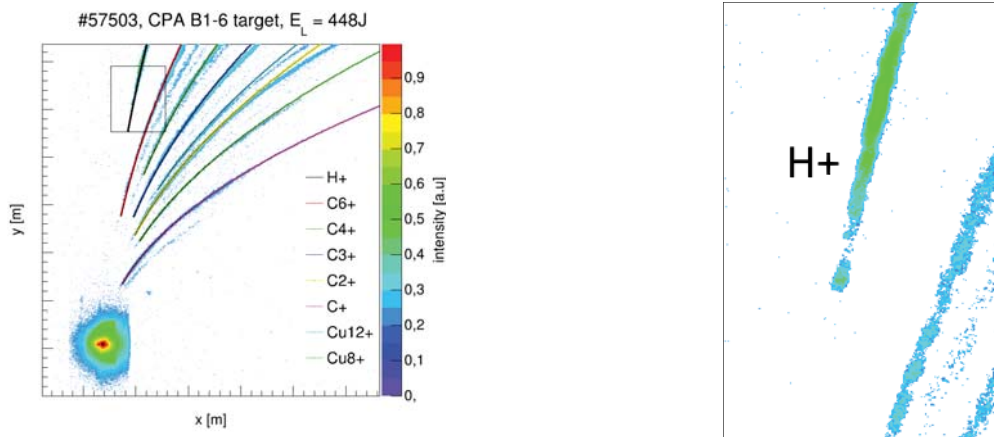

Fig. 8. Example of IP response for nonoptimal laser pointing inside the CPA target (left) and magnified region of the proton parabola (right).
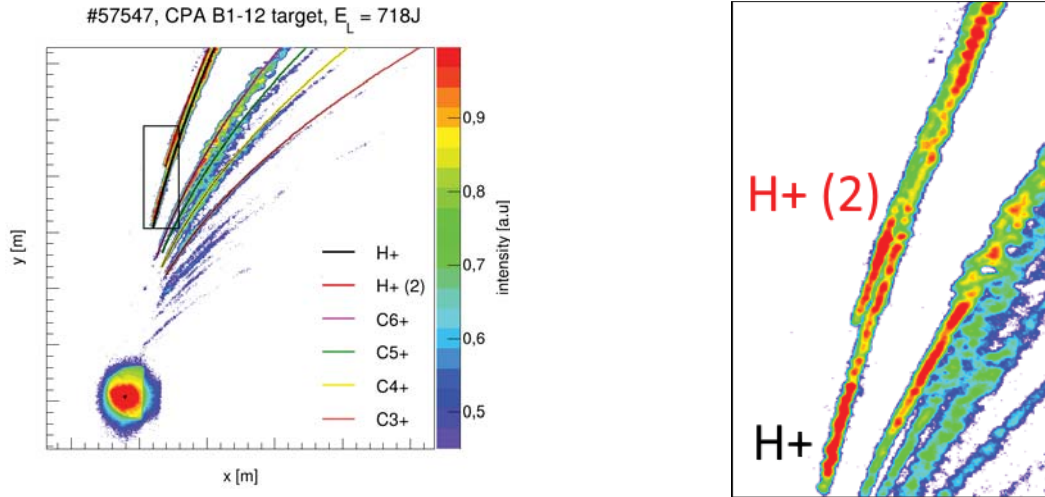
Fig. 9. Example of IP response for optimal laser pointing inside the CPA target (left) and the magnified region of the two visible proton parabolas (right).

of a visible secondary proton bunch, which is created during heating and pressurizing of the plasma confined in the cavity.

On the contrary, Fig. 9 displays the additional parabolic traces accompanying the initially ablated proton bunch, enhanced in both intensity and energy range of accelerated products, while the initial proton bunch exhibits properties similar to the case of nonideal laser guiding (Figs. 8 and 10). This is in agreement with the well-grounded observation of further acceleration of ions during the CPA scheme in terms of energy and increase of density of the plasma jet escaping the cavity after being compressed by thermal effects inside the target cavity [14].
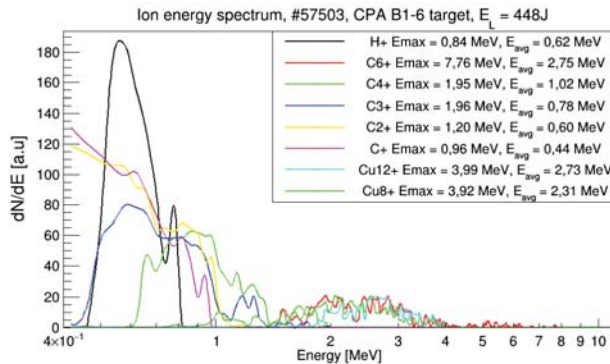
Fig. 10. Ion energy distribution for shot no. 57503.
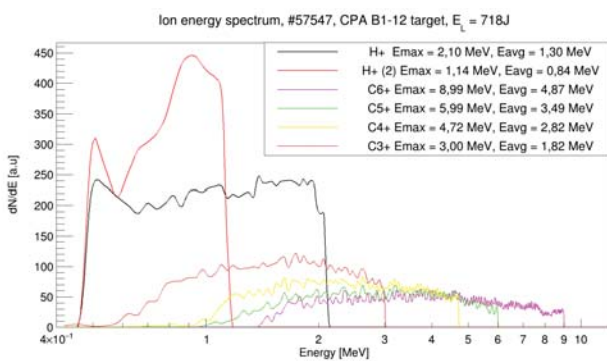
Fig. 11. Ion energy spectrum for the well-focused shot no. 57457.

The enhanced proton bunch (labeled as H+ in Figs. 9 and 11) is slightly displaced with respect to the initial proton signal (labeled as H+(2)) due to the difference in the path and origin of the accelerated products, as the ion jet created during the CPA scheme of acceleration is created and released from the cavity after heating and pressurizing the plasma inside the target. Our design of the Thomson spectrometer uses a single pinhole. Therefore, it behaves like a camera obscura and maps the position of the ion source. As a result, ions of the same type, which are accelerated during different processes and with different origins, are represented as separate parabolas.

Conclusion

The TPS designed in the IPPLM uses solid ferrite magnets with iron poles, together with electrodes in the wedge configuration, wherein the electric and magnetic deflection systems are not overlapping geometrically and are placed in series. This configuration allows application of lower voltages at the similar level of dispersion of deflected ions; hence, only one high-voltage power supply is required in contrast to the classical, parallel configuration. Moreover, since the magnetic separator is not overlapping with the electrodes, the gap between the iron poles can be minimized to obtain strong magnetic deflection while using moderately strong solid magnets instead of the electromagnet commonly used in the classic design of this kind of spectrometer. The possibility of accessible replacement of the detection system even during the experiment, coupled with the features mentioned above, ensures that our TPS can be easily adapted to different experimental setups on different laser systems.

The TPS used during the aforementioned experimental study revealed the uncommon nature of the acceleration process during the CPA process and, at the same time, allowed us to verify the proper laser guiding inside the CPA targets. We observed greatly enhanced (in terms of intensity) and approximately

doubled (in terms of maximum energy) secondary proton bunch accompanying the initially accelerated protons. Such results, even though qualitative due to the lack of calibration of the IP at the moment, explicitly confirm whether the expected formation of CPA-enhanced ion jet occurs in a given shot. Other commonly used diagnostic tools would not be able to provide this kind of information alone. Therefore, it confirms the assumption that using the TPS in novel approaches to laser–matter interaction is obligatory and allows us to greatly improve the understanding of processes that occur during the experiment.

ORCID

S. Borodziuk http://orcid.org/0000-0003-2340-4879
T. Chodukowski http://orcid.org/0000-0001-5835-1485
M. Rosiński http://orcid.org/0000-0002-3916-1122
M. Szymański http://orcid.org/0000-0001-6315-2421
P. Tchórz http://orcid.org/0000-0002-3674-607X

References

1. Donnan, F. G. (1923). Rays of positive electricity and their application to chemical analyses. By Sir J. J. Thomson, O. M. F. R. S. (2nd ed.). Pp. x + 237. London: Longmans, Green and Co., 1921. Price 16s. *Journal of the Society of Chemical Industry*, *42*(36), 861–861. https://doi.org/10.1002/JCTB.5000423614.

2. Daido, H., Nishiuchi, M., Pirozhkov, A. S., Fernández, J. C., Albright, B. J., Beg, F. N., & Badziak, J. (2018). Laser-driven ion acceleration: methods, challenges and prospects. *J. Phys.-Conf. Series*, *959*(1), 012001. https://doi.org/10.1088/1742-6596/959/1/012001.

3. Margarone, D., Krása, J., Giuffrida, L., Picciotto, A., Torrisi, L., Nowak, T., Musumeci, P., Velyhan, A., Prokůpek, J., Láska, L., Mocek, T., Ullschmied, J., & Rus, B. (2011). Full characterization of laser-accelerated ion beams using Faraday cup, silicon carbide, and single-crystal diamond detectors. *J. Appl. Phys.*, *109*, 103302. https://doi.org/10.1063/1.3585871.

4. Salvadori, M., Consoli, F., Verona, C., Cipriani, M., Anania, M. P., Andreoli, P. L., Antici, P., Bisesto, F., Costa, G., Cristofari, G., de Angelis, R., di Giorgio, G., Ferrario, M., Galletti, M., Giulietti, D., Migliorati, M., Pompili, R., & Zigler, A. (2021). Accurate spectra for high energy ions by advanced time-of-flight diamond-detector schemes in experiments with high energy and intensity lasers. *Sci. Rep.*, *11*(1), 1–16. https://doi.org/10.1038/s41598-021-82655-w.

5. Raczka, P., Nowosielski, L., Rosiński, M., Makaruk, D., Makowski, J., Zaraś-Szydłowska, A., Tchórz, P., & Badziak, J. (2019). Measurement of the electric field strength generated in the experimental chamber by 10 TW femtosecond laser pulse interaction with a solid target. *J. Instrum.*, *14*(04). https://doi.org/10.1088/1748-0221/14/04/P04008.

6. Carroll, D. C., Brummitt, P., Neely, D., Lindau, F., Lundh, O., Wahlström, C. G., & McKenna, P. (2010). A modified Thomson parabola spectrometer for high resolution multi-MeV ion measurements-Application to laser-driven ion acceleration. *Nucl. Instrum. Methods Phys. Res.-Sect. A-Accel. Spectrom. Dect. Assoc. Equ.*, *620*(1), 23–27. https://doi.org/10.1016/J.NIMA.2010.01.054.

7. Wagner, F., Deppert, O., Brabetz, C., Fiala, P., Kleinschmidt, A., Poth, P., Schanz, V. A., Tebartz, A., Zielbauer, B., Roth, M., Stöhlker, T., & Bagnoud, V. (2016). Maximum proton energy above 85 MeV from the relativistic interaction of laser pulses with micrometer thick CH_2 targets. *Phys. Rev. Lett.*, *116*, 205002. https://doi.org/10.1103/PhysRevLett.116.205002.

8. Alejo, A., Gwynne, D., Doria, D., Ahmed, H., Carroll, D. C., Clarke, R. J., Neely, D., Scott, G. G., Borghesi, M., & Kar, S. (2016). Recent developments in the Thomson parabola spectrometer diagnostic for laser-driven multi-species ion sources. *J. Instrum.*, *11*(10), C10005. https://doi.org/10.1088/1748-0221/11/10/C10005.

9. Kojima, S., Inoue, S., Hung Dinh, T., Hasegawa, N., Mori, M., Sakaki, H., Yamamoto, Y., Sasaki, T., Shiokawa, K., Kondo, K., Yamanaka, T., Hashida, M., Sakabe, S., Nishikino, M., & Kondo, K. (2020). Compact Thomson parabola spectrometer with variability of energy range and measurability of angular distribution for low-energy laser-driven accelerated ions *Rev. Sci. Instrum.*, *91*, 53305. https://doi.org/10.1063/5.0005450.

10. Woryna, E., Parys, P., Wołowski, J., & Mróz, W. (1996). Corpuscular diagnostics and processing methods applied in investigations of laser-produced plasma as a source of highly ionized ions. *Laser Part. Beams*, *14*(3), 293–321. https://doi.org/10.1017/S0263034600010053.

11. Jungwirth, K., Cejnarova, A., Juha, L., Kralikova, B., Krasa, J., Krousky, E., Krupickova, P., Laska, L., Masek, K., Mocek, T., Pfeifer, M., Präg, A., Renner, O., Rohlena, K., Rus, B., Skala, J., Straka, P., & Ullschmied, J. (2001). The Prague Asterix Laser System. *Phys. Plasmas*, *8*, 2495. https://doi.org/10.1063/1.1350569.

12. Chodukowski, T., Borodziuk, S., Rusiniak, Z., Cikhardt, J., Jach, K., Krasa, J., Rosinski, M., Terwinska, D., Dudzak, R., Pisarczyk, T., Swierczynski, R.,

Burian, T., Tchorz, P., Dostal, J., Szymanski, M., Pfeifer, M., Skala, J., Singh, S., Krupka, M., & Krus, M. (2020). Neutron production in cavity pressure acceleration of plasma objects. *AIP Adv.*, *10*(8), 085206. https://doi.org/10.1063/5.0005977.

13. Green, B. D., & Goela, J. S. (1986). Ablative acceleration of small particles to high velocity by focused laser radiation. *JOSA B*, *3*(1), 8–14. https://doi.org/10.1364/JOSAB.3.000008.

14. Borodziuk, S., Kasperczuk, A., & Pisarczyk, T. (2009). Cavity pressure acceleration: An efficient laser-based method of production of high-velocity macroparticles. *Appl. Phys. Lett.*, *95*, 231501. https://doi.org/10.1063/1.3271693.